Supporting Information for

Solvent-Controlled Ion-Coupled Charge Transport in Microporous Metal Chalcogenides

Jacob McKenzie, Paul A. Kempler, and Carl K. Brozek*

Department of Chemistry and Biochemistry,

Materials Science Institute, Oregon Center for Electrochemistry

University of Oregon, Eugene, OR 97403

Email: cbrozek@uoregon.edu

Table of Contents

Experimental Methods

Materials. All commercial chemicals were used as received unless stated otherwise. Germanium powder (99.99%, Sigma Aldrich), sublimed sulfur powder (99%, Strem), tetramethylammonium hydroxide pentahydrate (95%, Oakwood Chemical), iron(II) chloride (anhydrous, Strem), zinc(II) nitrate hexahydrate (98%, Sigma Aldrich), hexanes (98.5%, Fisher Chemical), toluene (99.5%, Fisher Chemical), chloroform (99.9%, Fisher Chemical), tetrahydrofuran (99.9%, Oakwood Chemical), dichloromethane (99.5%, Fisher Chemical), *tert*-butanol (99%, J.T. Baker), 2-propanol (99%, Fisher Scientific), *n*-propanol (Macron Chemicals, 99%), acetone (≥99.5%, Fisher Chemical), ethanol ((200 proof, Decon Labs), methanol (99.8%, Fisher Chemical), formamide (Fisher Chemical, 99.5%), 1,2-dichlorobenzene (≥99%, Fisher Scientific) and nanopure water (Thermo Scientific, Barnstead Nanopure). Solvothermal syntheses were conducted in autoclave PAAR bombs in Yamato Convection oven unless stated otherwise.

Characterization. Sample purity and crystallinity was verified by powder X-ray diffraction (PXRD) with a Bruker D2 Phaser benchtop diffractometer.

Dry Pressed pellet conductivity measurements. Pressed pellets were prepared by compressing powders in a modified KBr pellet press die set with a hydraulic press at 500 psi for 30 minutes. The pellet press die set was modified with tinned copper wires affixed to both sides with silver paint and epoxy. Electrical contacts were made by pressing a pellet with the modified die set comprised of stainless-steel circular ends serving as two electrode contacts. Direct-current (DC) conductivities were determined from the slopes of current-voltage (*I-V*) curves collected with a GAMRY Instruments Interface 5000E potentiostat, along with the electrode area (0.402 cm^2) and pellet thickness, according to the equation below (where *C* is the slope of the most linear portion of the *I-V* curve and *m* is the pellet thickness):

$$DC_\sigma : \frac{C * m}{0.402}$$

The associated error for conductivity measurements was found by compounding errors from both the pellet dimensions (*m* and the electrode area) and the linear regression analysis used to find C, using the following equation [where Δm is the error associated with the pellet thickness (0.002 cm, from the precision of the digital calipers utilized) Δa is the error associated with the electrode area (0.0045 cm^2) and ΔC is the error associated with the linear regression performed to obtain the slope:

$$\Delta DC_\sigma = DC_\sigma \left(\frac{\Delta m}{m} + \frac{\Delta a}{0.402} + \frac{\Delta C}{C} \right)$$

Unless specified otherwise, samples were swept voltammetrically at 2 mV/s between –0.2/(-0.1) and 0.1 V vs OCP compressed by a C-clamp. Temperature-dependent measurements were conducted in a similar fashion with samples kept at fixed temperatures in a Yamato Convection oven.

Pressed pellet conductivity measurements after solvent addition. Pressed pellets were prepared as described above. To the prepared pellets 10 μL of a solvent were added and the OCP was monitored to determine stability. Direct-current (DC) conductivities were determined from the

slopes of the most linear portion of the current-voltage (I-V) curves collected with a GAMRY Instruments Interface 5000E potentiostat, along with the electrode area (0.402 cm^2) and pellet thickness, according to the equation above. Temperature dependent measurements were conducted in a similar fashion with samples kept at fixed temperatures in a Yamato Convection oven.

Dry pressed pellet EIS measurements. Using a setup identical to the pressed pellet conductivity measurements, AC measurements were run with a DC voltage of 0 V vs. OCP with an AC amplitude of 50 mV and 300 mV for TMA$_2$FeGe$_4$S$_{10}$ and TMA$_2$ZnGe$_4$S$_{10}$ respectively, from 2 MHz to 0.1 Hz.

Solvent dependent pressed pellet EIS measurements (TMA$_2$FeGe$_4$S$_{10}$). Using a setup identical to the pressed pellet conductivity measurements, AC measurements were run with a DC voltage of 0 V vs. OCP from 2 MHz to 0.1 (0.01) Hz after the addition of 10 μL of a solvent. An AC voltage of 50 mV was employed for CH$_2$Cl$_2$, IPA, *n*-propanol, and EtOH; and 10 mV was the AC voltage for MeOH and deionized water. OCP was allowed to stabilize before beginning measurements.

Solvent dependent pressed pellet EIS measurements (TMA$_2$ZnGe$_4$S$_{10}$). Using a setup identical to the pressed pellet conductivity measurements, AC measurements were run with a DC voltage of 0 V vs. OCP from 2 MHz to 0.1 Hz after the addition of 10 μL of a solvent. An AC voltage of 50 mV was employed for CH$_2$Cl$_2$, IPA, *n*-propanol, EtOH, MeOH and deionized water. OCP was allowed to stabilize before beginning measurements.

Synthetic Procedures

Precursor Cluster Syntheses

TMA₄Ge₄S₁₀. Following a procedure outlined in our previous report,[1] germanium powder (1 g, 13.76 mmol), sulfur powder (1.77 g, 6.88 mmol), and water (7.44 g, 412.8 mmol) were added to a Teflon Parr bomb. While slowly stirring this mixture with a glass rod, tetramethyl ammonium hydroxide pentahydrate (4.99 g, 27.5 mmol) was added and then the Parr bomb was sealed and placed in a fixed-temperature oven at 150 °C for 15 hours. The resulting yellow solution was vacuum filtered to remove unreacted germanium and then ~500 ml of acetone was added to induce precipitation of a white solid. The white powder was washed with acetone (20 ml ×3), hot toluene (20 ml ×3), and hexanes (20 ml ×3), then dried overnight under dynamic vacuum to afford an off-white powder. The resulting product was stored under ambient conditions.
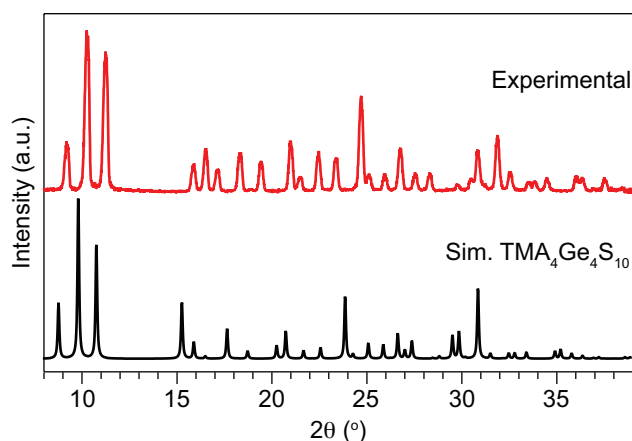

Figure S1: Experimental (red trace) and simulated (black trace) powder X-ray diffraction patterns of $TMA_4Ge_4S_{10}$.

TMA₂MGe₄S₁₀ (M = Fe, Zn) Syntheses

All procedures were followed as outlined in our previous report.[1]

TMA₂FeGe₄S₁₀: Anhydrous iron(II) chloride (0.050 g, 0.40 mmol) and TMA₄Ge₄S₁₀ (0.18 g, 0.20 mmol) were dissolved in 4 ml and 8 ml of N₂-sparged DI water, respectively under positive nitrogen atmosphere. The iron solution was added dropwise to the TMA₄Ge₄S₁₀ solution over the course of ~2 minutes. The solution was allowed to react at room temperature for ~12 hours. The bright-orange solid was washed with sparged DI water (15 ml × 2), ethanol (15 ml × 2), and hexanes (15 ml × 2) sequentially. Then, the solid was dried with a stream of nitrogen and stored under positive N₂ atmosphere.

TMA₂ZnGe₄S₁₀. Zinc(II) nitrate hexahydrate (0.12 g, 0.40 mmol) and TMA₄Ge₄S₁₀ (0.18 g, 0.20 mmol) were dissolved in 4 and 8 ml of DI water, respectively. The zinc solution was added dropwise to the TMA₄Ge₄S₁₀ solution over the course of ~2 minutes. The resulting solution was left to react at room temperature for ~12 hours. The white solid was washed with DI water (15 ml × 3) and then dried in a fixed temperature oven at 150 °C for ~12 hours. The resulting material was stored under ambient conditions.
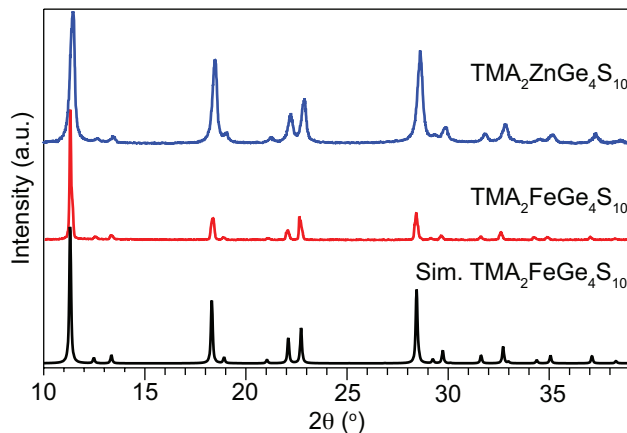
Figure S2: Experimental powder X-ray diffraction patterns for $TMA_2MGe_4S_{10}$ (M: Fe and Zn) compared against a simulated pattern of $TMA_2FeGe_4S_{10}$.

DC Electrochemical Analyses

Diffusion coefficients were obtained by plotting the current from chronoamperometry experiments vs. the sqrt(t) and utilizing the equation below (where n is number of electrons (1), F is Faraday's constant, D_0 is the diffusion coefficient, C_0 is the concentration of TMA^+, and A (0.402 cm^2) is the area of the electrode). The concentration of TMA^+ was calculated given the crystal structure for $TMA_2FeGe_4S_{10}$.[2]

$$i(t) = \frac{nFAD_0C_0}{\pi^{1/2}t^{1/2}}$$

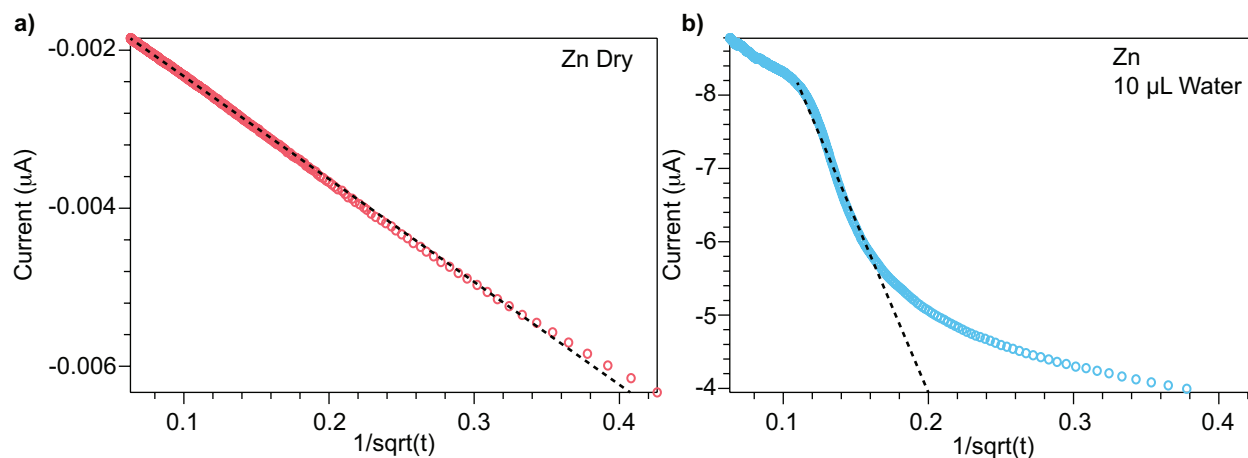**Figure S3:** Cottrell plots for the current transients obtained at -0.2V of a pressed pellet of $TMA_2ZnGe_4S_{10}$ before (a) and after (b) the addition of 10 µL of deionized water. The dotted trace fits are used to obtain diffusion coefficients.

S5

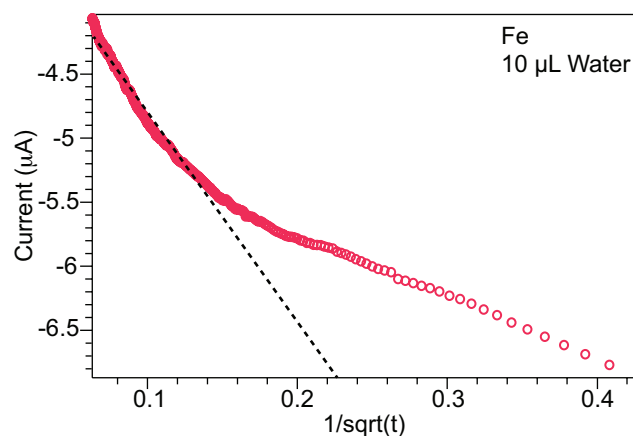**Figure S5:** Cottrell plots for the current transients obtained at -0.2V for a pressed pellet of TMA$_2$FeGe$_4$S$_{10}$ after addition of 10 μL of deionized water. The dotted trace fits are used to obtain diffusion coefficients.
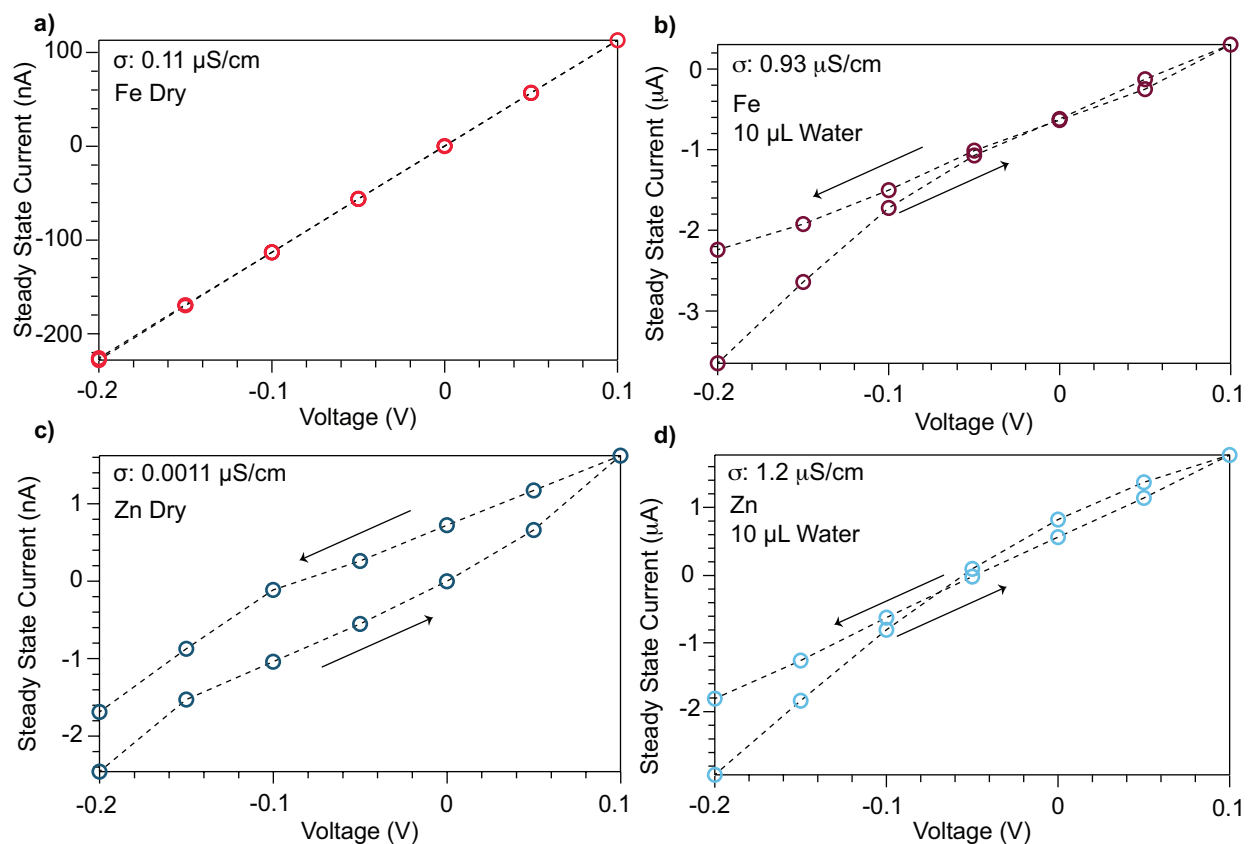

Figure S4: Steady-state current values vs. applied potential derived from chronoamperometry experiments for pressed pellets of TMA$_2$FeGe$_4$S$_{10}$ before (a) and after (b) the addition of 10μL of deionized water and pressed pellets of TMA$_2$ZnGe$_4$S$_{10}$ before (c) and after the addition of 10μL of deionized water (d). Arrows denote the direction of potential scanned. Conductivity values are displayed and calculated from the slope of the return scan.
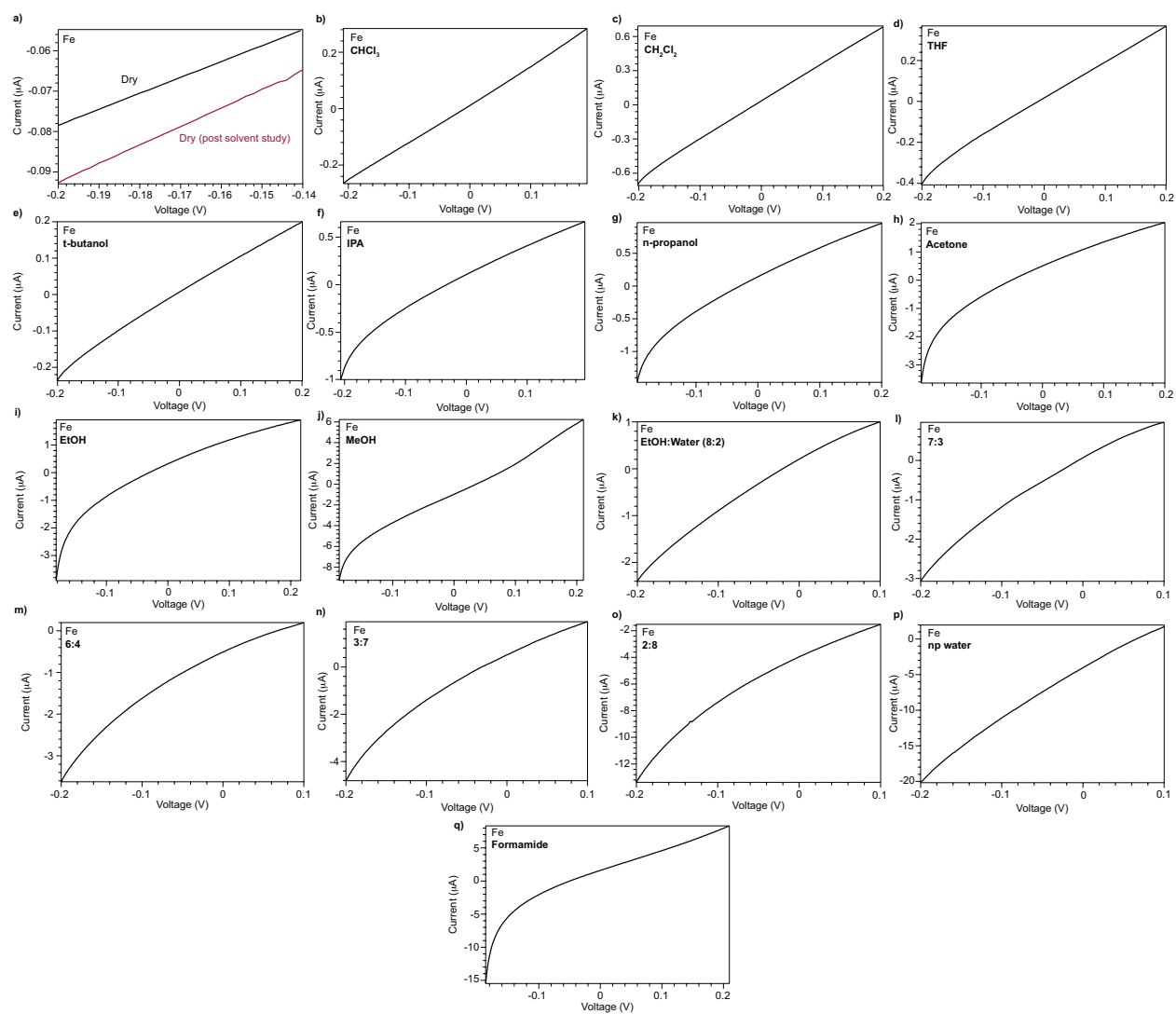
Figure S6: *I-V* curves measured for pressed-pellets of $TMA_2FeGe_4S_{10}$ scanned at 2mV/s subjected to various conditions: Dry (a), $CHCl_3$ (b), CH_2Cl_2 (c), THF (d), *t*-butanol (e), IPA (f), *n*-propanol (g), acetone (h), EtOH (i), MeOH (j) EtOH:Water mixtures [8:2 (k), 7:3 (l), 6:4 (m), 3:7 (n), 2:8 (o)], deionized water (p), and formamide (q).
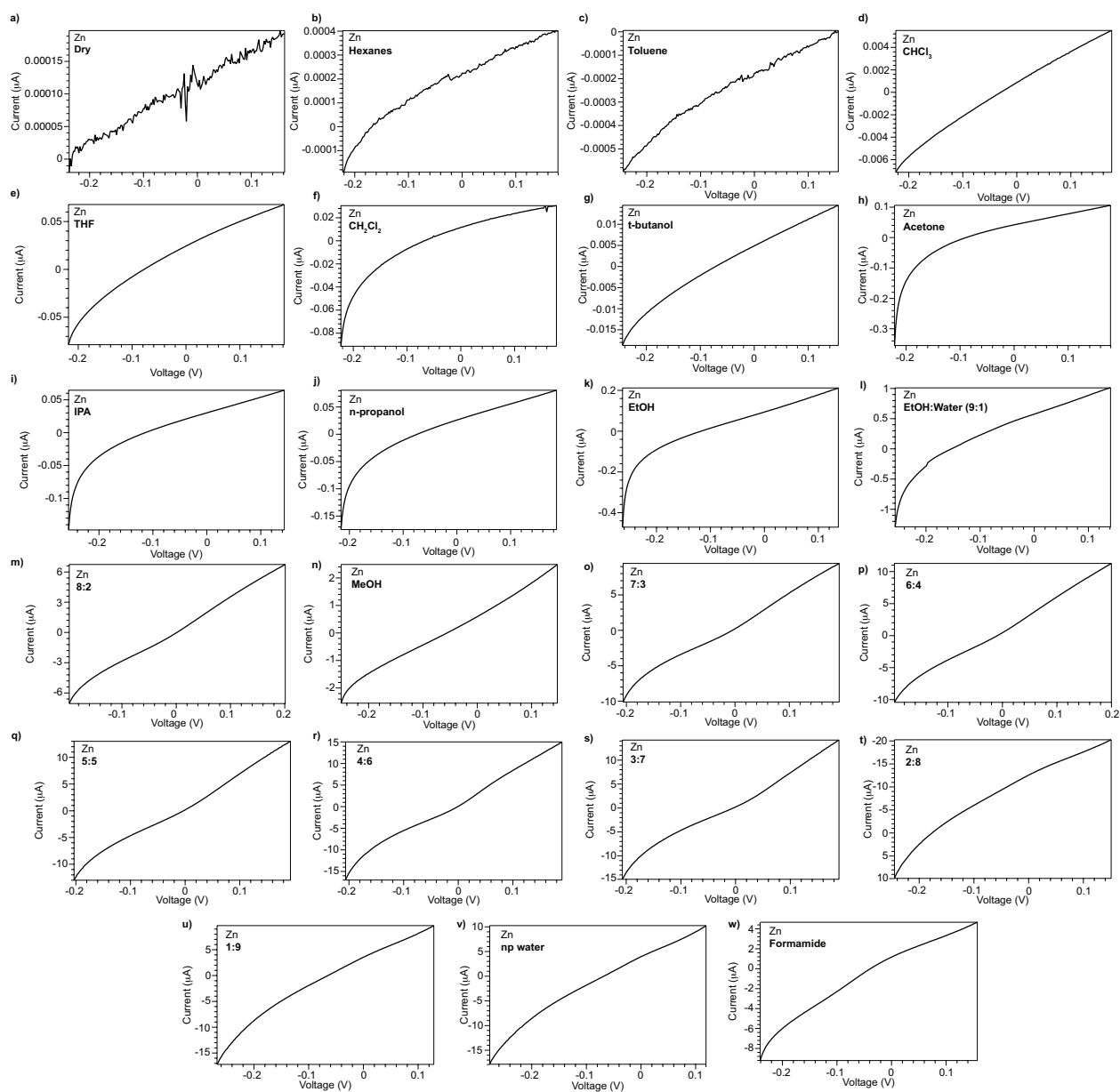
Figure S7: *I-V* curves for pressed pellets of TMA$_2$ZnGe$_4$S$_{10}$ scanned at 2mV/s subjected to various conditions: Dry (a), hexanes (b), toluene (c), CHCl$_3$ (d), THF (e), CH$_2$Cl$_2$ (f), *t*-butanol (g), acetone (h), IPA (i), *n*-propanol (j), EtOH (k), MeOH (n) EtOH:Water mixtures [9:1 (l). 8:2 (m), 7:3 (o), 6:4 (p), 5:5 (q), 4:6 (r), 3:7 (s), 2:8 (t), 1:9 (u)], deionized water (v), and formamide (w).
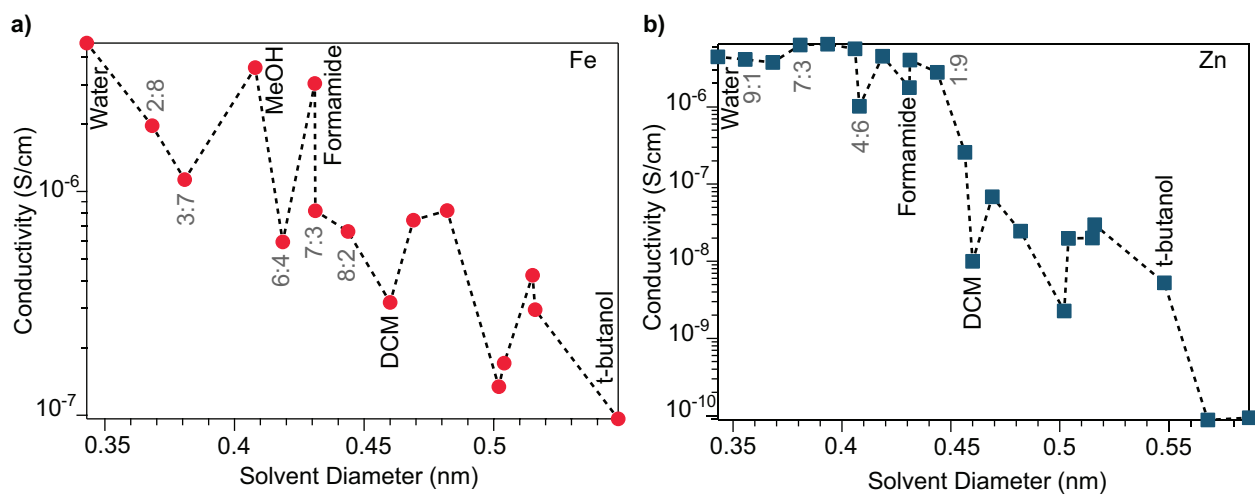
Figure S8: Solvent-dependent DC conductivity values of $TMA_2FeGe_4S_{10}$ (a) and $TMA_2ZnGe_4S_{10}$ (b) pressed-pellets obtained from linear fits to *I-V* curves swept voltammetrically between –0.2 V and 0.2 V. The conductivity values are plotted vs. solvent size

Electrochemical Impedance Analysis

All EIS fits were performed using the open source EIS Spectrum Analyzer.[3] To fit an equivalent circuit, a circuit was first built given the EIS response and knowledge of the material and experimental constraints (e.g. use of ion blocking electrodes), then equivalent circuits were fit using the Powell algorithm using the amplitude function.
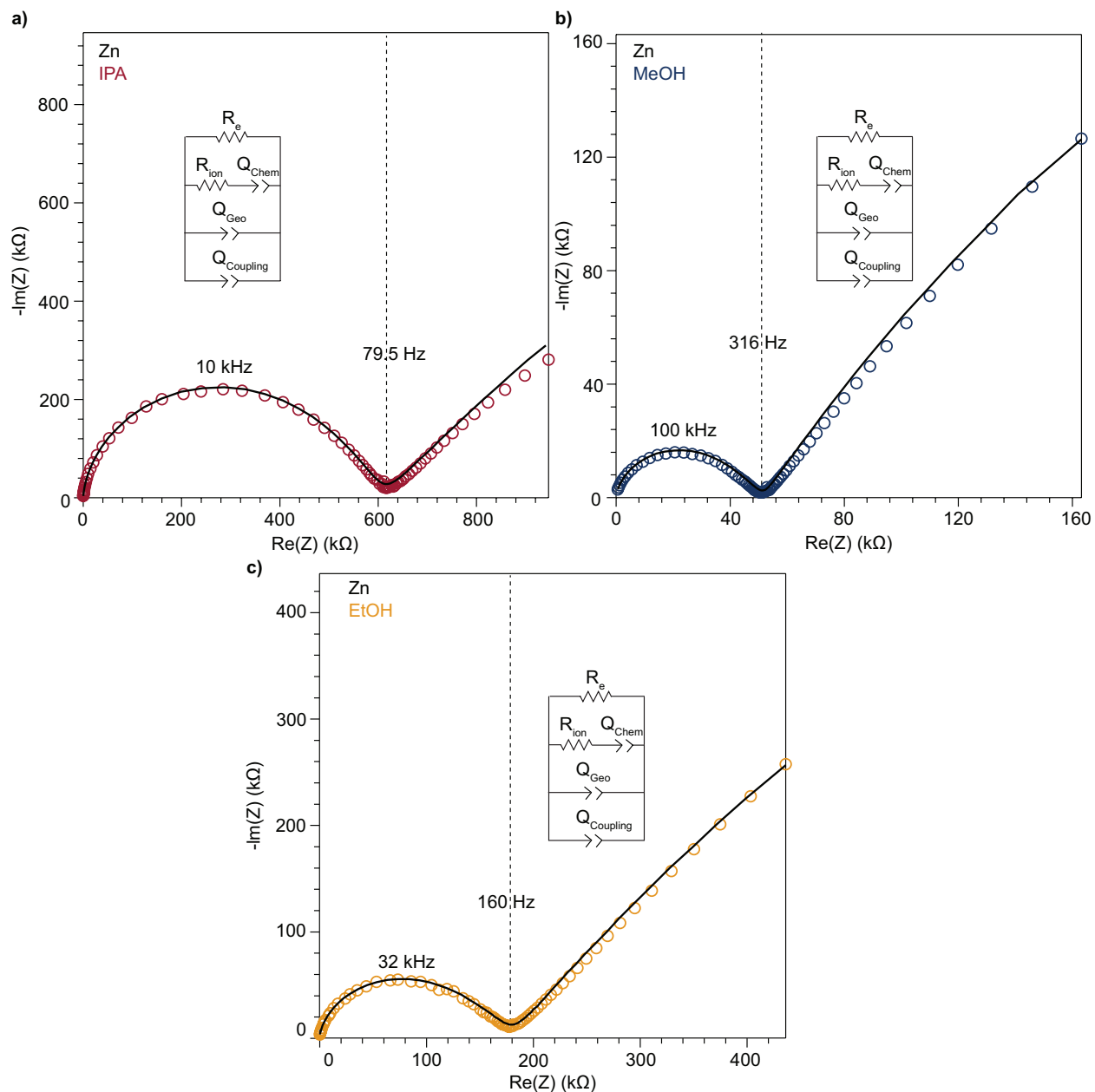
Figure S9: Nyquist plots of $TMA_2ZnGe_4S_{10}$ pressed-pellets after addition of IPA **(a)**, MeOH **(b)**, and EtOH **(c)**. Black traces represent fits to the equivalent circuit diagrams shown in the figure
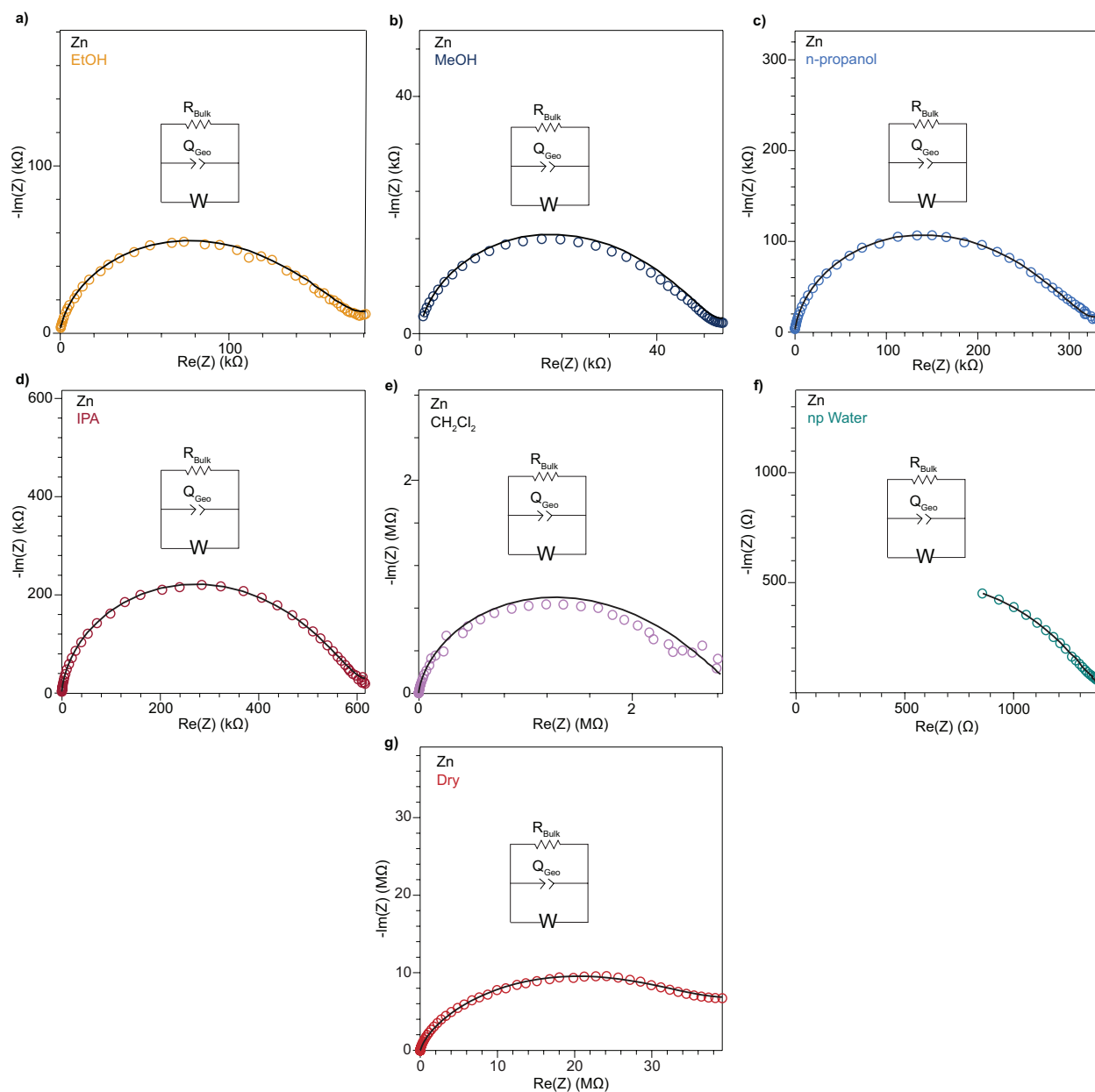
Figure S10: Nyquist plots of $TMA_2ZnGe_4S_{10}$ pressed-pellets focused on the high frequency domain after addition of EtOH **(a)**, MeOH **(b)**, *n*-propanol **(c)**, IPA **(d)**, CH_2Cl_2 **(e)**, deionized water **(f)**, and dry **(g)**. Black traces represent fits to the displayed equivalent circuit diagrams and emphasize the effect of replacing a CPE for a Warburg element.
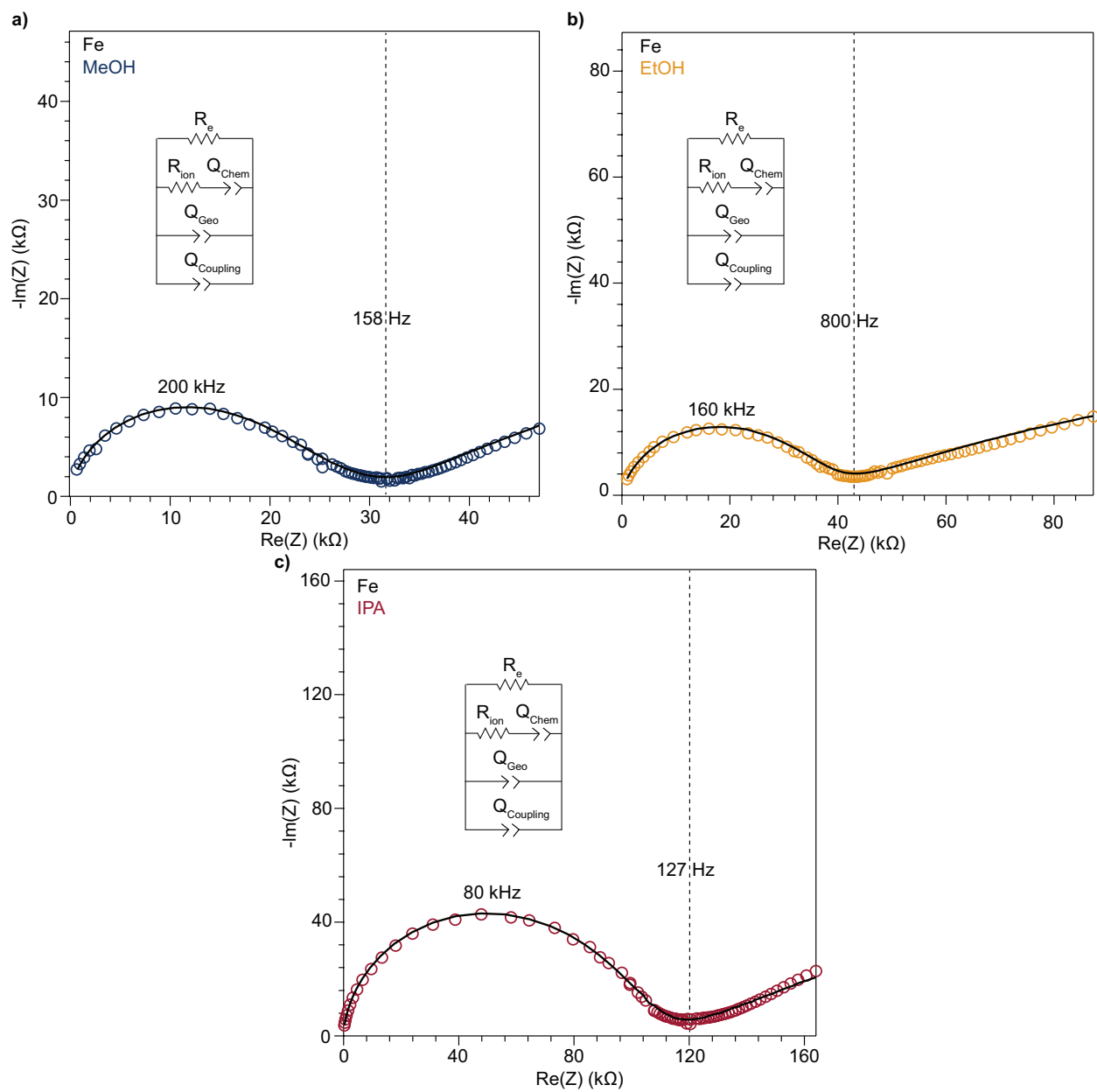
Figure S11: Nyquist plots of TMA$_2$FeGe$_4$S$_{10}$ pressed-pellets after addition of MeOH **(a)**, EtOH **(b)**, and IPA **(c)**. Black traces represent fits to the equivalent circuit diagrams shown in the figure.
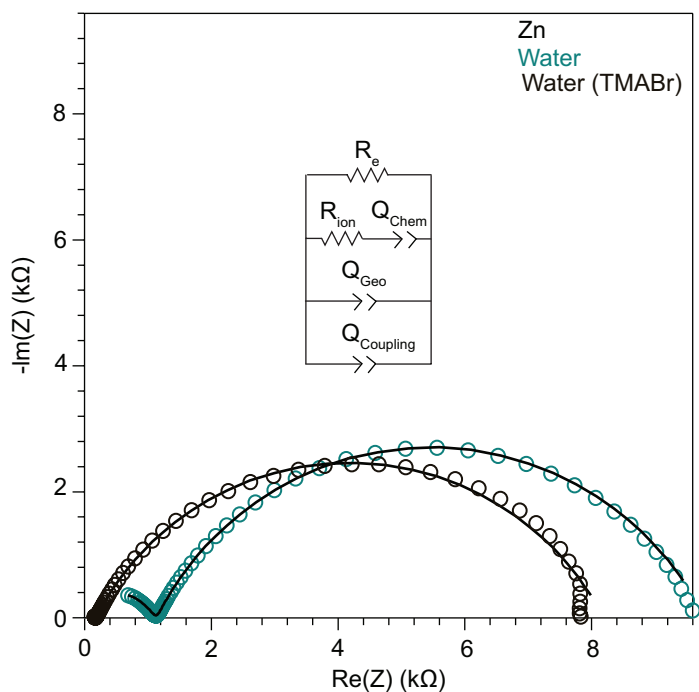
Figure S12: Nyquist plots of $TMA_2ZnGe_4S_{10}$ pressed-pellets after addition of deionized water **(a)**, and a 0.1-M TMABr aqueous solution **(b)**. Black traces represent fits to the equivalent circuit diagram shown in the figure.
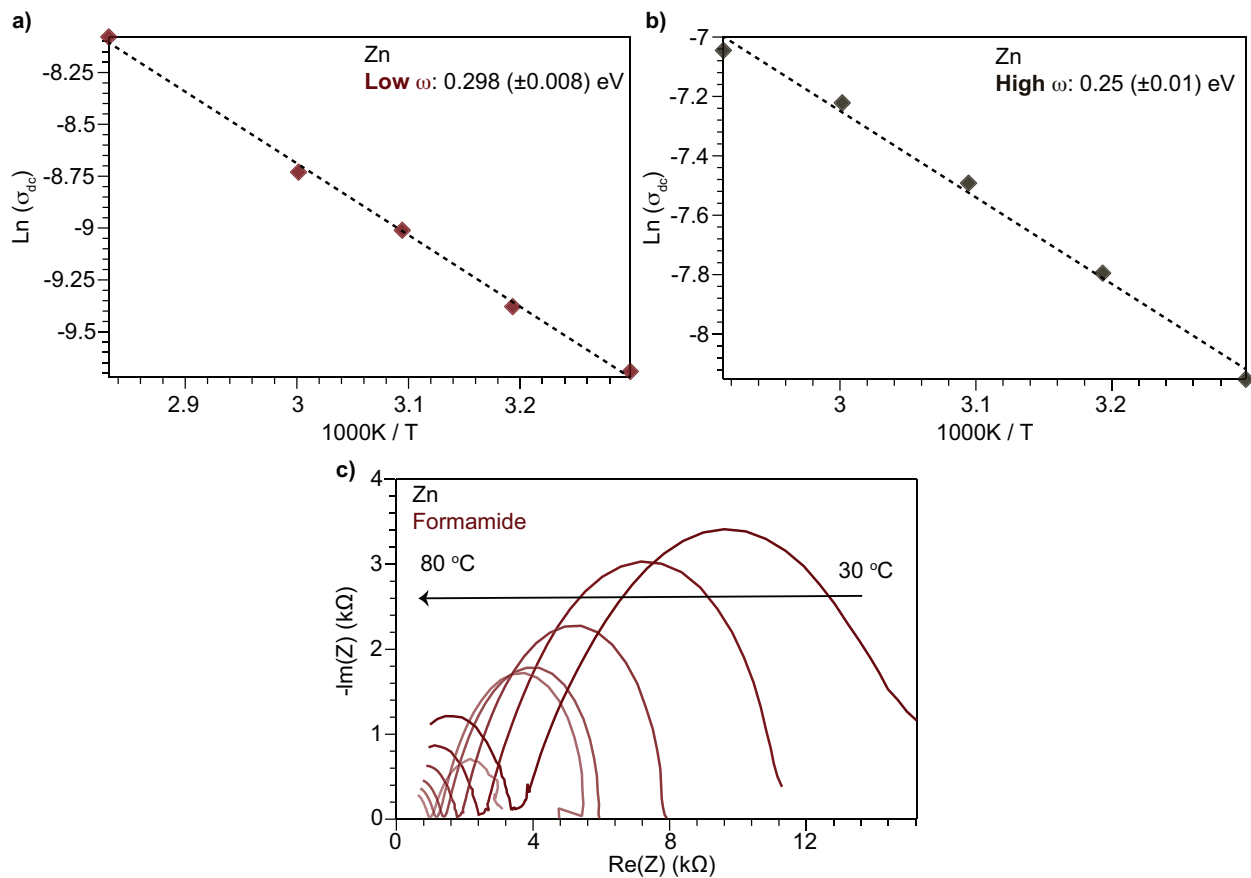
Figure S13: Arrhenius plots for the low (**a**) and high (**b**) frequency *x*-intercept resistances from temperature-dependent EIS performed on pressed pellets of $TMA_2ZnGe_4S_{10}$ after formamide treatment (**c**).

Left section

Solvent	Circuit Element	Fitted Value	Error (%)
n-propanol	Bulk Q	$0.039\ nS.S^n$	1.16
	n		
	Chemical Q	$19\ \mu S.S^n$	3.65
	n	0.31	4.24
	Ionic Resistance	$87\ k\Omega$	2.54
	Electronic Resistance	$395\ k\Omega$	2.54
	Coupling Q	$0.12\ \mu S.S^n$	3.5
	n	0.3	0.96
IPA	Bulk Q	$0.025\ nS.S^n$	1.32
	n	0.99	0.089
	Chemical Q	$16\ \mu S.S^n$	4.74
	n	0.27	5.95
	Ionic Resistance	$132\ k\Omega$	0.84
	Electronic Resistance	$0.092\ M\Omega$	4.63
	Coupling Q	$27\ nS.S^n$	5.2
	n	0.37	1.09
MeOH	Bulk Q	$0.063\ nS.S^n$	2.07
	n	0.95	0.14
	Chemical Q	$39\ \mu S.S^n$	5.74
	n	0.32	6.5
	Ionic Resistance	$42\ k\Omega$	1.16
	Electronic Resistance	$145\ k\Omega$	3.07
	Coupling Q	$0.35\ \mu S.S^n$	3.5
	n	0.3	0.9
EtOH	Bulk Q	$0.032\ nS.S^n$	2.15
	n	0.97	0.14
	Chemical Q	$12\ \mu S.S^n$	2.23
	n	0.25	2.22
	Ionic Resistance	$44\ k\Omega$	1.12
	Electronic Resistance	$240\ k\Omega$	2.7
	Coupling Q	$11\ nS.S^n$	2.97
	n	0.54	0.38

Right section

Solvent	Circuit Element	Fitted Value	Error (%)
Water	Bulk Q	$0.074\ nS.S^n$	7.99
	n	1	0.48
	Chemical Q	$77\ \mu S.S^n$	2.31
	n	0.4	1.45
	Ionic Resistance	$1.3\ k\Omega$	1.39
	Electronic Resistance	N/A	N/A
	Coupling Q	$33\ \mu S.S^n$	4.3
	n	0.15	3.17
	Contact Resistance	$200\ \Omega$	0.4
DCM	Bulk Q	$0.042\ nS.S^n$	1.16
	n	0.96	0.08
	Chemical Q	N/A	N/A
	n	N/A	N/A
	Ionic Resistance	N/A	N/A
	Electronic Resistance	$449\ k\Omega$	0.86
	Coupling Q	$8.2\ nS.S^n$	2.6
	n	0.29	0.86
Dry	Bulk Q	$0.036\ nS.S^n$	1.3
	n	0.97	0.09
	Chemical Q	N/A	N/A
	n	N/A	N/A
	Ionic Resistance	N/A	N/A
	Electronic Resistance	$1.13\ M\Omega$	0.93
	Coupling Q	$7.8\ nS.S^n$	6.5
	n	0.37	1.7

Table S1: Equivalent circuit fit parameters and their associated percent error for pressed pellet EIS performed on $TMA_2FeGe_4S_{10}$.

Solvent	Circuit Element	Fitted Value	Error (%)	Solvent	Circuit Element	Fitted Value	Error (%)
n-propanol	Bulk Q	$0.022\ nS.S^n$	1.69	*DCM*	Bulk Q	$0.030\ nS.S^n$	2.5
	n	1	0.12		n	0.98	0.18
	Chemical Q	$3.2\ \mu S.S^n$	4.7		Chemical Q	N/A	N/A
	n	0.6	3.97		n	N/A	N/A
	Ionic Resistance	373 kΩ	1.12		Ionic Resistance	3.1 MΩ	3.3
	Electronic Resistance	3.22 MΩ	8.1		Electronic Resistance	N/A	N/A
	Coupling Q	$8.4\ nS.S^n$	3.89		Coupling Q	$4.3\ nS.S^n$	6.7
	n	0.48	0.66		n	0.45	1.5
IPA	Bulk Q	$0.022\ nS.S^n$	1.23	*Water*	Bulk Q	$0.051\ nS.S^n$	5.75
	n	1	0.09		n	1	0.35
	Chemical Q	$2.4\ \mu S.S^n$	4.29		Chemical Q	$20\ \mu S.S^n$	1.4
	n	0.52	4.2		n	0.71	0.46
	Ionic Resistance	686 kΩ	0.91		Ionic Resistance	1.1 kΩ	0.74
	Electronic Resistance	5.93 MΩ	6.7		Electronic Resistance	9.6 kΩ	0.97
	Coupling Q	$2.2\ nS.S^n$	4.1		Coupling Q	$0.46\ \mu S.S^n$	5.9
	n	0.55	0.6		n	0.41	0.93
					Contact Resistance	150 Ω	3.6
MeOH	Bulk Q	$0.031\ nS.S^n$	3.2	*w/ TMABr*	Bulk Q	N/A	N/A
	n	0.98	0.21		n	N/A	N/A
	Chemical Q	$7\ \mu S.S^n$	3.53		Chemical Q	$31\ \mu S.S^n$	1
	n	0.62	2.6		n	0.7	0.3
	Ionic Resistance	55 kΩ	1.39		Ionic Resistance	180 Ω	1.02
	Electronic Resistance	1.03 MΩ	5.2		Electronic Resistance	8.2 kΩ	0.93
	Coupling Q	$22\ nS.S^n$	5.7		Coupling Q	$0.32\ \mu S.S^n$	10.8
	n	0.48	0.84		n	0.5	1.3
EtOH	Bulk Q	$0.021\ nS.S^n$	2.35	*Dry*	Bulk Q	$0.028\ nS.S^n$	5.6
	n	1	0.16		n	1	0.8
	Chemical Q	$3\ \mu S.S^n$	3.6		Chemical Q	$0.13\ \mu S.S^n$	2
	n	0.56	2.96		n	0.4	2.4
	Ionic Resistance	193 kΩ	1.3		Ionic Resistance	40 MΩ	0.37
	Electronic Resistance	1.84 MΩ	3.75		Electronic Resistance	N/A	N/A
	Coupling Q	$11\ nS.S^n$	3.99		Coupling Q	$2.8\ nS.S^n$	6.7
	n	0.5	0.62		n	0.48	0.44

Table S2: Equivalent circuit fit parameters and their associated percent error for pressed pellet EIS performed on $TMA_2FeGe_4S_{10}$.
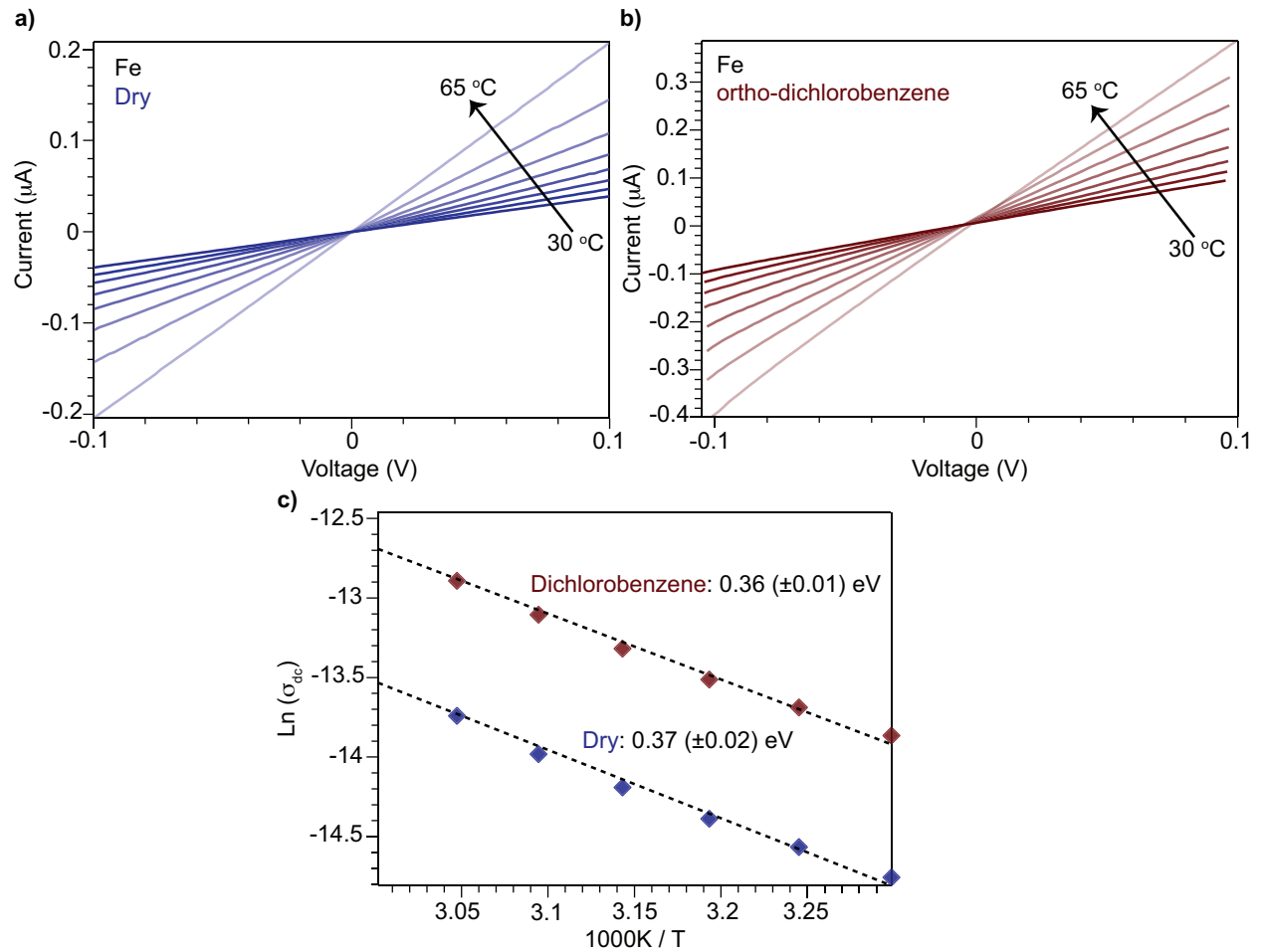
Temperature Dependent DC Conductivity

Figure S14: *I-V* curves for pressed pellets of $TMA_2FeGe_4S_{10}$ scanned at 2mV/s from 30 - 65 °C before (a) and after (b) the addition of ortho-dichlorobenzene. Arrhenius fits (dotted traces) provide electronic conduction activation barriers for dry (blue) and ortho-dichlorobenzene (red).
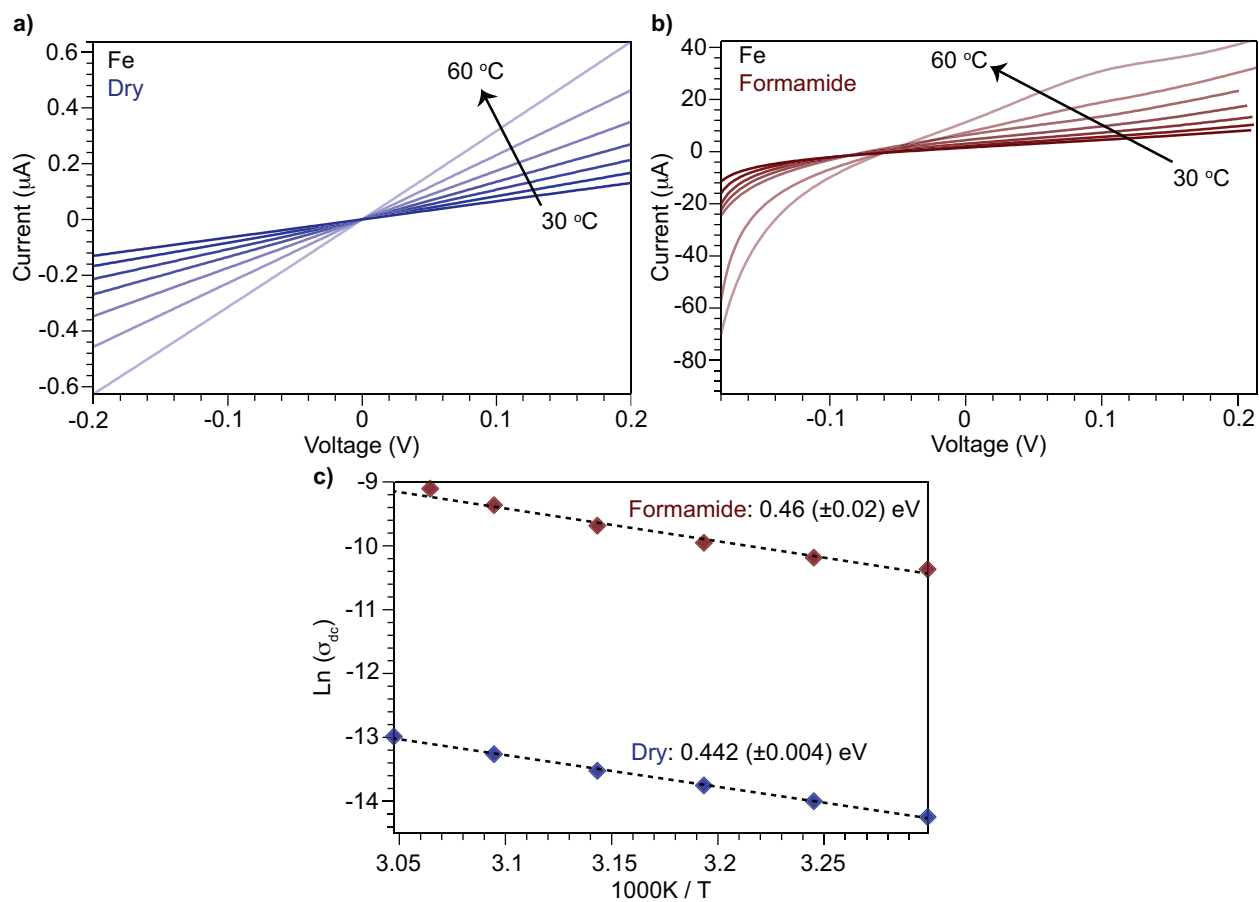
Figure S15: *I-V* curves for pressed pellets of TMA$_2$FeGe$_4$S$_{10}$ scanned at 2mV/s from 30 - 65 °C before (a) and after (b) the addition of formamide. Arrhenius fits (dotted traces) provide electronic conduction activation barriers for dry (blue) and or (red).

References

(1)   McKenzie, J.; Le, K. N.; Bardgett, D. J.; Collins, K. A.; Ericson, T.; Wojnar, M. K.; Chouinard, J.; Golledge, S.; Cozzolino, A. F.; Johnson, D. C.; Hendon, C. H.; Brozek, C. K. "Conductivity in Open-Framework Chalcogenides Tuned via Band Engineering and Redox Chemistry." *Chem. Mater.* **2022**, *34* (4), 1905–1920. https://doi.org/10.1021/acs.chemmater.1c04285.

(2)   Bowes, C. L.; Lough, A. J.; Malek, A.; Ozin, G. A.; Petrov, S.; Young, D. "Thermally Stable Self-Assembling Open-Frameworks: Isostructural Cs^+ and $(CH_3)_4N^+$ Iron Germanium Sulfides." *Chem. Ber.* **1996**, *129* (3), 283–287. https://doi.org/10.1002/cber.19961290307.

(3)   Bondarenko A. S., Ragoisha G. A. *EIS Spectrum Analyser*; In Progress in Chemometrics Research, Pomerantsev A. L., Ed.; Nova Science Publishers: New York, 2005.